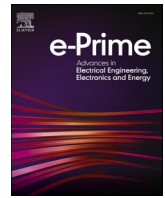




Contents lists available at ScienceDirect

# e-Prime - Advances in Electrical Engineering, Electronics and Energy

journal homepage: [www.elsevier.com/locate/prime](http://www.elsevier.com/locate/prime)

## Energy-autonomous UHF RFID sensor for tire pressure monitoring system

Julien Sourice<sup>a</sup>, Gilbert Kaboré<sup>a</sup>, Nathan Sauger<sup>a</sup>, Abdelaziz Hamdoun<sup>a,b</sup>,  
Mohamed Latrach<sup>a,b,\*</sup>

<sup>a</sup> ESEO, 10 Boulevard Jean Jeanneteau, Angers 49100, France

<sup>b</sup> RF-EMC Research Group, ESEO, IETR UMR CNRS 6164, 10 Boulevard Jean Jeanneteau, Angers 49100, France

### ARTICLE INFO

#### Keywords:

Pressure monitoring system  
Radio frequency identification  
Power harvester  
Passive smart-tag  
Electric bike  
Rectenna

### ABSTRACT

Thanks to the miniaturization of components and therefore the significant reduction of energy needs, the design of passive smart-tag incorporating intelligent sensors is now possible. The goal of this study is to develop a tire pressure sensor for an electric bike with battery-free. Therefore, there is no need to replace periodically the battery, so as cuts off maintenance costs and extend the life time of the smart-tags. An UHF RFID reader installed on the bicycle frame and connected to the battery e-bike transmits the RF power at 868 MHz toward each tag integrated in the wheel rims.

Firstly, this article presents the whole hardware architecture of a passive smart-tag which had to respond of technics constraints and the complexity to integrate 2 antennas in a small package box. Secondly, the methods to ensure an ultra-low consumption are developed. Finally, practical tests are compared with simulations, and, validations are carried out showing the compliance and the industrialization of this innovative system.

### 1. Introduction

A large part of the sensors cannot be powered by an embedded battery alone, as many applications are difficult to access. Furthermore, experts predict that 22 billion IoT devices will be commercialized by 2025 [1]. Devices whose sensor constitutes the main element and therefore a necessary need to improve its energy autonomy. Such an improvement will allow the extension of the functional life of the device, reduce the toxic waste of the batteries and reduce the size.

The development of this study falls within this context and concerns the design of an RFID tire pressure detection system, helpful for an electric bicycle. The goal is to provide a preventive solution for its user in order to guarantee its safety but also to ensure the operating status of this vehicle, for example, interesting for a fleet of rental bikes. The smart RFID sensors tag is designed to work without battery and to demonstrate a new design approach than existing TPMS (Tire Pressure Monitoring System).

The system developed<sup>1</sup> consists of an UHF RFID reader and two passive RFID sensors tags intended to be placed inside the wheels. In today's market, there are only TPMS operating at 433 MHz and requiring battery power, such as a button cell that needs to be replaced

every time the tires need to be changed. Consequently, our aim is to design an innovative system which will provide a competitive solution.

This paper is organized as follows: Section 2 presents the details of our approach and the different technical choices, results and discussions developed in Section 3 illustrate the theoretical and experimental validation of our study, while comments and conclusions are presented in Section 4.

### 2. Design approach and components choice

The RFID TPMS developed is composed of a passive smart sensors tag using the EPC global GEN2 protocol and the SparkFun Simultaneous RFID Reader - M6E-Nano [2] with a Data transfer in half-duplex mode. This mode allows data exchange, between the tag and the reader, and energy recovery when the tag is close to the reader. Therefore, a smart sensor tag is placed on each wheel rim (Fig. 1) and attached to it to be independent of the tire constraints. The compatible tires are only tubeless type. After each wheel tour, it turned out that the presence of tag in the very close area to the RFID reader, made it possible to harvest enough electrical energy to be able to store it.

The developed tag is composed of two hardware main parts (Fig. 2),

\* Corresponding author at: ESEO, 10 Boulevard Jean Jeanneteau, Angers 49100, France.

E-mail address: [mohamed.latrach@eseo.fr](mailto:mohamed.latrach@eseo.fr) (M. Latrach).

<sup>1</sup> Study carried out by Julien, Gilbert and Nathan, in 120 h, in the framework of the RFID Projects, for ESEO\* Engineering Students, under the supervision of Mohamed LATRACH.(\*) ESEO : Ecole Supérieure d'Electronique de l'Ouest, Angers, France

<https://doi.org/10.1016/j.prime.2022.100072>

Received 27 July 2022; Received in revised form 5 September 2022; Accepted 22 September 2022

Available online 28 September 2022

2772-6711/© 2022 The Authors. Published by Elsevier Ltd. This is an open access article under the CC BY license (<http://creativecommons.org/licenses/by/4.0/>).

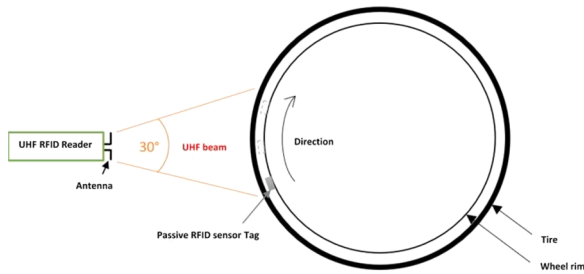


Fig. 1. Tag implantation synoptic on the bicycle wheel.

the first is dedicated to harvest and manage the energy; and the second is intended for data collection, processing and wireless sending.

2.1. Antenna designs

The first sub-assembly is designed with an antenna for harvesting the electrical energy at 868 MHz. It can be the reader signal or another RF sources which transmit on the same frequency, from -10 dBm to 5 dBm of the RF/DC converter sensibility.

Next, a RF/DC module converts the captured RF signal into continuous power. This step is realized by a specific module of reference P2110B [3] of PowerCast manufacturer. This power harvester circuit is able to transform the electromagnetic energy in power supply and boosted the level at 3.3 V for ensuring compliant voltage. In order to define the antenna specifications to be connected to the P2110B input, a study was carried out to meet the requirements of the RF energy harvesting device.

The IFA antenna topology choice [4] seems to be the most appropriate in this study, given its miniature size (Fig. 3) and an appropriate operating frequency band (frequency bandwidth and gain are respectively around 30 MHz and 2 dBi). The optimum antenna size obtained by the Momentum/ADS software is 75 mm by 40 mm. A high-Q DC blocking capacitor is added in series with this antenna for its connecting to the P2110B input access.

For energy storage, a supercapacitor is defined. Indeed its benefits are multiple, such as a low Equivalent Series Resistance (ESR), a fast charging ability, a longer cycle life (superior to 500 000 electric loads and unloads) and the smaller size. The capacity size was calculated according the P2110B specifications and the active mode time to have sufficient energy. This made it possible to choose the BZ055B153ZSB capacitor [5] manufactured by AVX Corporation.

The second main part concerns the microcontroller and its peripherals. It is part of ultra-low power microcontroller family manufactured by ST [6] (Reference: STM32L031K6T7, 1 mA in active mode and 3.2 μA in sleep mode) and it supervises the power supply to the: pressure and temperature sensor [7] (Reference: MS5803, Manufacturer: TE Connectivity) and an RFID chip EPC Gen2 interface [8] (Reference: SL3S4021, Manufacturer: NXP).

The temperature sensor provides a temperature accuracy inferior to 0.01 °C on a scale from -20 to +85 °C, and the pressure sensor sets a value between 0 and 7 bar with of an accuracy of 0.1 bar. The temperature combined with the pressure are analyzed by the microcontroller to improve a wheel' pressure detection. As soon as the wheel starts to turn, the system wakes up automatically every 30 s during 40 ms and updates the RFID chip register with the new pressure value. The smart-tag and the reader are asynchronous. Indeed, the smart-tag gives access to his register for allowing the reader to read the data.

If the pressure value is less than a critical level defined in the RFID reader software, a beep is emitted to warn the bicycle user. Otherwise, the microcontroller returns to standby mode to save power.

To establish the communication up to the wheel diameter, the antenna connected on the RFID chip must have sufficient gain to reduce the RF power emitted by the RFID reader and to be compatible with the

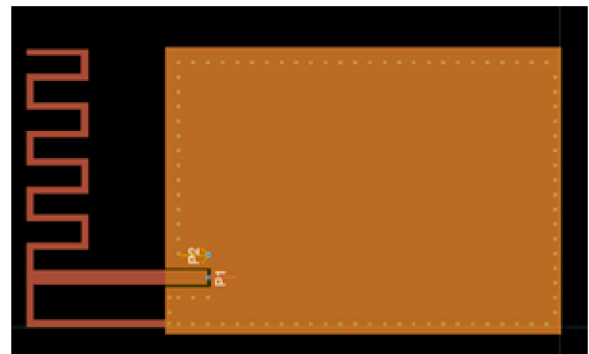


Fig. 3. Designed IFA antenna (75 × 40 mm<sup>2</sup>).

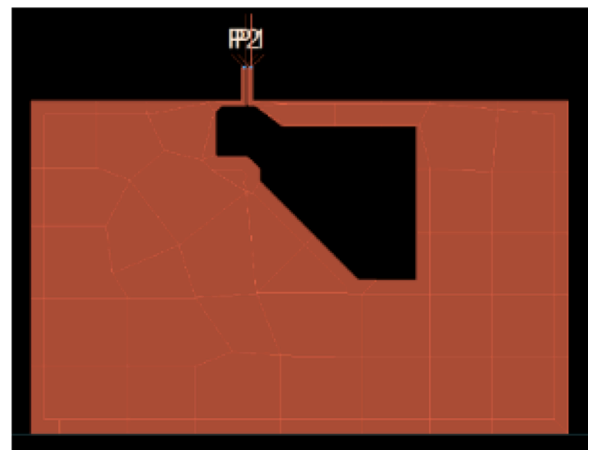


Fig. 4. Designed Slot antenna (30 × 40 mm<sup>2</sup>).

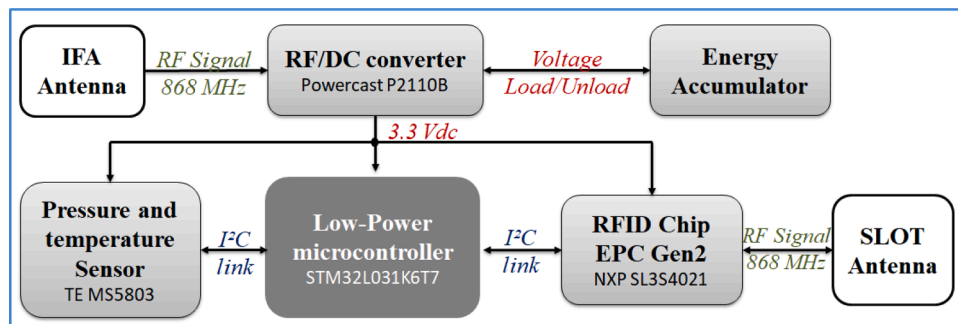


Fig. 2. Passive smart sensor tag synoptic.



Fig. 5. Smart-tag prototype (respectively IFA on the left and slot antenna on the right).

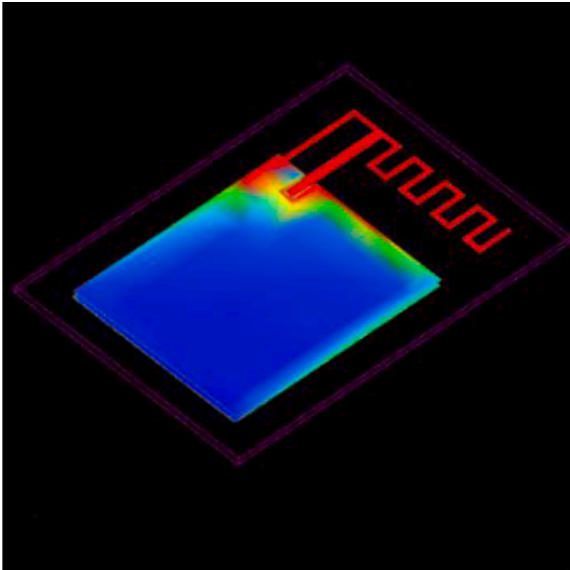


Fig. 6. Screenshot of simulated surface current distribution at 868 MHz under Momentum/ADS.

bike and with the bicycle' metal structure. This second antenna (Fig. 4) is a slot antenna allowing data exchange between the RFID chip and the reader. It is designed on a single PCB with obtained simulated gain of 2 dBi. With the presented specifications in the NXP application note [9], the antenna conductive area must be wide for better performance, however, the final PCB size to be designed depends on the bicycle rim' width. Thus, in this study case, the PCB size to be carried out must not exceed an area of  $40 \times 120 \text{ mm}^2$ .

The two PCB antennas have a linear polarization and their arrangement, on the PCB ((Figs. 5& 9), has been defined to minimize their mutual coupling. Consequently, the principal polarization plan of the first antenna is oriented perpendicularly to the second antenna. Moreover, a distance of  $\lambda/2$  between the two antennas is held. In addition, the areas not colored in dark blue in Fig. 6 are forbidden to the locations of EMI<sup>2</sup>-sensitive electronics.

### 2.2. Components choice

The temperature and pressure sensor choice is defined by the low consumption current and the particularly benefit of owned a converter analogic/numeric which is already calibrated and which returns an accurate numeric value by reading on I2C-bus standard, on the contrary, an analogic sensor should have calibrated before using.

The choice of the RFID chip interface EPC Gen2 is based on the low consumption current ( $40 \mu\text{A}$  in I<sup>2</sup>C write mode), the sensitivity reception ( $-18 \text{ dBm}$  in read mode), the low package size (QFN10 type) and the capacity to communicate with this chip by I2C-bus.

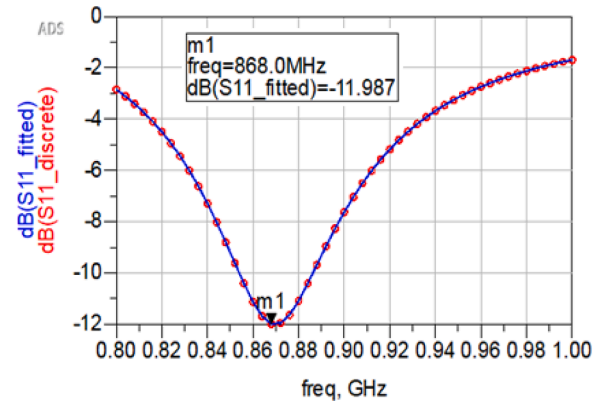


Fig. 7. Simulated reflection coefficient response of the IFA.

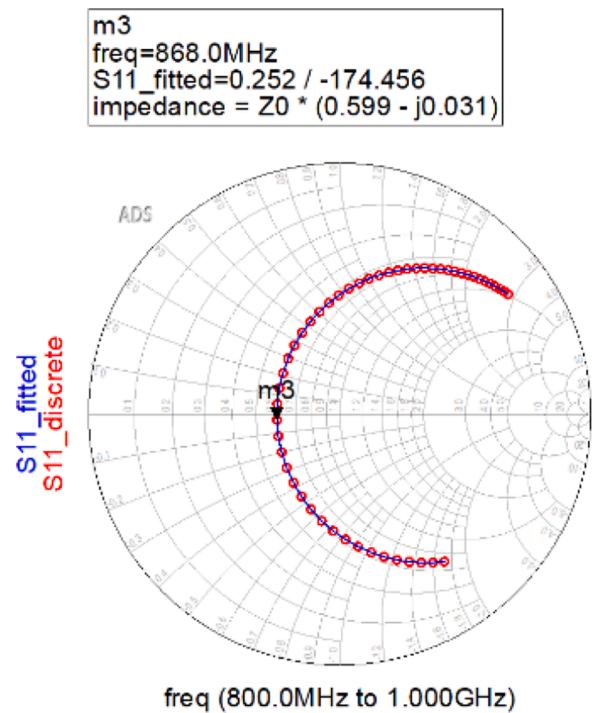


Fig. 8. Simulated input impedance of the IFA.

## 3. Experimental data analysis and results

In this section will be presented both simulation and experimental results of the two antennas and the test results of the power harvester (rectenna) system connected to the storage capacitor. The simulations of the antennas were done on Advance Design System (ADS) software of Keysight technologies.

### 3.1. Simulation and experimental study of the IFA antenna

The Fig. 7 shows the return loss  $S_{11}$  parameter. The obtained resonant frequency is 868 MHz at a return loss of  $-11.98 \text{ dB}$ ; the bandwidth is 20 MHz. The phase shift is close to  $-180^\circ$ .

This antenna is feed by microstrip line with characteristic impedance of  $50 \Omega$ . Fig. 8 shows that the simulated input impedance of the designed IFA is  $30 \Omega$  and matches the input impedance of the used power harvester chip.

At 868 MHz, the simulated efficiency and gain are 83.7% and 1.41 dBi, respectively. The polarization of this antenna is vertical.

In order to measure the electrical characteristics of the designed IFA,

<sup>2</sup> EMI : Electromagnetic interference

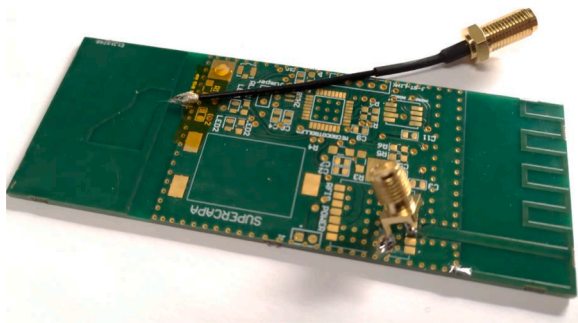


Fig. 9. SMA connector and coaxial cable soldered respectively to the feed point of IFA and slot antenna.

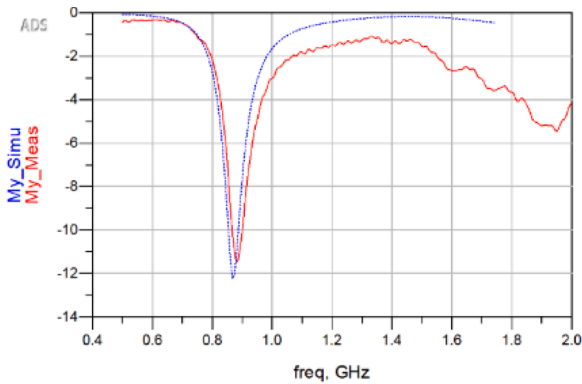


Fig. 10. Comparison between simulated and measured reflection coefficient of the IFA.

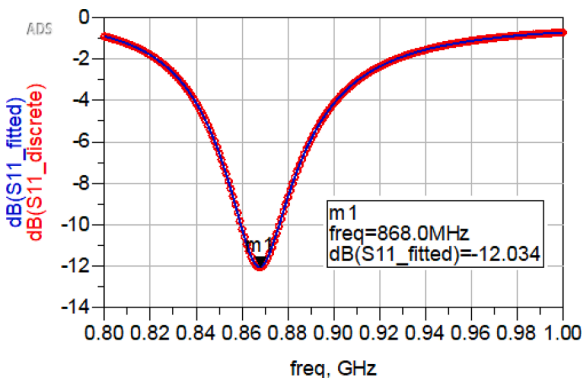


Fig. 11. Simulated reflection coefficient response of the slot antenna.

an SMA connector was soldered to its feed point as shown in the Fig. 9. And thanks to a network analyzer with port adapted in 50 Ω, the reflection coefficient ( $\| S_{11} \|$ ) has been measured on the bandwidth from 0.4 GHz to 2 GHz.

The measured return loss of the IFA is shown in Fig. 10, by the red curve, and the simulation result is shown by the blue curve. A good concordance between simulation and measurement results is observed. The observed frequency small offset is due to the integration of the SMA connector.

### 3.2. Simulation and experimental study of the slot antenna

The simulation results of the slot antenna reflection coefficient ( $\| S_{11} \|$ ) can be seen in Fig. 11 and its input impedance can be simulated also as shown in Fig. 12.

m3  
 freq=866.0MHz  
 $S_{11\_fitted}=0.253 / 178.068$   
 impedance =  $Z_0 * (0.596 + j0.011)$

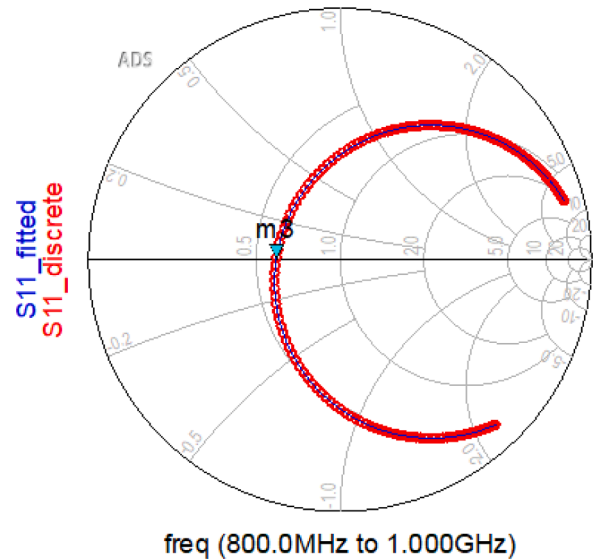


Fig. 12. Simulated input impedance of the slot antenna.

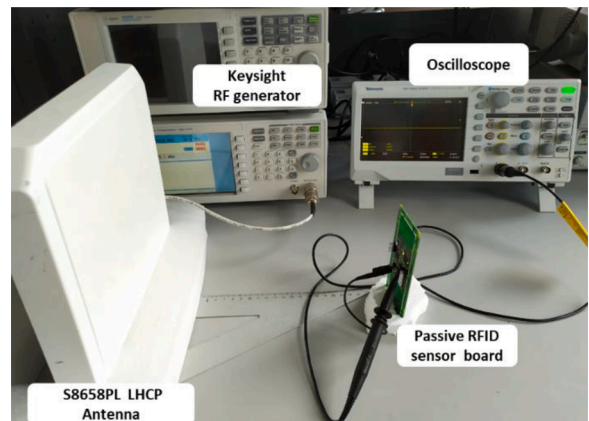


Fig. 13. Test bench of supercapacitor charging and discharging measurement.

From this simulation we can see that the antenna reflection coefficient is  $-12.00$  dB at 868 MHz.

At the same frequency of 868 MHz the antenna input impedance is  $50 * (0.59 + j0.011) \Omega$ , the gain is  $-0.5$  dBi and the radiation efficiency is 28.2%.

For this antenna, the experimental measurement of the reflection coefficient could not be verified because the network analyzer input impedance was unsuitable and requires a microscopic differential probe.

So, a check with the whole operational system was carried out under real conditions. The measured reception distance, between 40 mm and 170 mm, ensures the compliance of the designer slot antenna.

### 3.3. Power harvester measurement

In this section we will report on measurement made on the RF/DC power conversion system (Fig. 13). Using an N9310 KEYSIGHT RF generator, we transmit a 20 dBm signal at 868 MHz (ASK modulation) with 8 dBi S8658PL LHCP transmitting antenna. We place the prototype board at 250 mm away from this antenna in the same scenario as the use

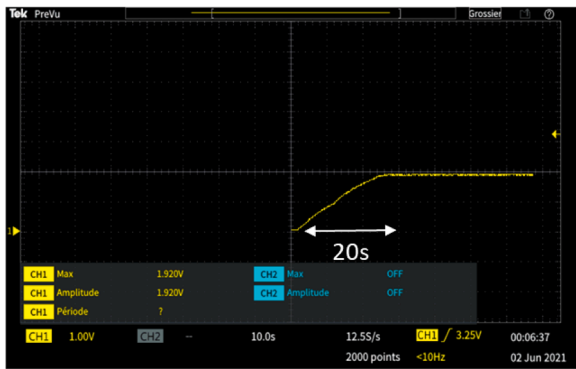


Fig. 14. Accumulator (supercapacitor) charging time measurement.

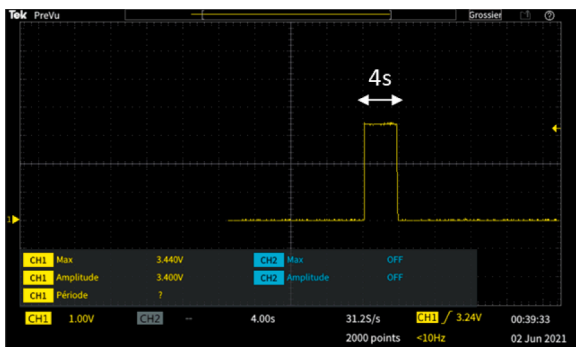


Fig. 15. Accumulator (supercapacitor) discharge time measurement.

intended on the e-bike. With a line-of-sight transmission, the full charge time measured of the supercapacitor is about 20 s (Fig. 14).

According to the exposure time of the IFA antenna to EM radiation per wheel revolution, the time required to charge the capacitor is calculated. In our study case, it takes about 300 turns for a full charge of the capacitor.

In order to check whether the stored energy is sufficient for our system, a 3.3 kΩ resistor is placed in series with the smart-tag power supply output to simulate an equivalent load to the consumption of our system (microcontroller + all peripherals). So, an oscilloscope is used to measure in continuous the supercapacitor voltage (Figs. 13& 14). This test indicates the time it takes for the capacitor to fully discharge under the minimum voltage required to operate the system as if it was supplied continuously.

Thus, the supercapacitor allows a power source of 3.3 V at 1 mA for about 4 s (Fig. 15). It meets our expectations since it provides 50 measurements of temperature and pressure.

The reduction in transmission power may cause an increase in the supercapacitor charging time and/or a reduction in the communication range between the base station and the sensor positions.

#### 4. Conclusion

This study presents the designing of a passive TPMS intended to control the tire pressure on an electric bike. The developed RFID passive smart sensors tag is operational and can harvest the energy sent by an RFID reader with a minimum of 4 dBm receiving signal.

His-algorithm triggers the measures of sensors and sequences the sleep and active modes. To obtain a better accuracy of the pressure, a measurement of the temperature is additionally done by the microcontroller. Every 30 s, the measurement is updated in the RFID chip memory, allowing the RFID reader to warn the e-bike user if the pressure drops (accuracy temperature  $\pm 0.5$  °C, accuracy pressure  $\pm 0.5$  bar).

The growing need for autonomous embedded systems in many

domains requires new research and approaches to develop more suitable and sustainable systems.

The main perspectives are the research of another method to measure the slot antenna return loss, to increase antennas gain; and firmware improvement to optimize the current consumption and the system autonomy. Finally, a complete study will have to be done to check the compliance of all the results and to carry out the industrialization of this study system.

#### Declaration of Competing Interest

The authors declare that they have no known competing financial interests or personal relationships that could have appeared to influence the work reported in this paper

#### References

- [1] K.L. Lueth, "State of the IoT 2020" Nov 2020, <https://iot-analytics.com>.
- [2] SparkFun, SEN-14066, [https://cdn.sparkfun.com/assets/4/e/5/5/0/SEN-14066\\_datasheet.pdf](https://cdn.sparkfun.com/assets/4/e/5/5/0/SEN-14066_datasheet.pdf), September 17, 2018.
- [3] PowerCast, P2110B, <https://www.powercastco.com/wp-content/uploads/2016/12/P2110B-Datasheet-Rev-3.pdf>, December 2016.
- [4] Fredrik KERVEL, Design note DN023, Post Office Box 655303, TEXAS 75265, Texas Instruments Incorporated, 2011.
- [5] AVX, BZ055B153ZSB, <http://catalogs.avx.com/BestCap.pdf>, 2019.
- [6] ST-MicroElectronics, STM32L031K6T7, <https://www.st.com/resource/en/datasheet/stm32l031k6.pdf>, March 2018.
- [7] TE CONNECTIVITY, MS5803-01BA, [https://www.te.com/commerce/DocumentDelivery/ENG\\_DS\\_MS5803-01BA\\_B3.pdf](https://www.te.com/commerce/DocumentDelivery/ENG_DS_MS5803-01BA_B3.pdf), June 2017.
- [8] NXP, SL3S4021, <https://www.nxp.com/part/SL3S4021FHK.pdf>, September 2018.
- [9] AN11180, Company public NXP, High Tech Campus 46, 5656 AE Eindhoven, October 24, 2012.



Julien SOURICE is an electronics student-engineer at École Supérieure d'Électronique de l'Ouest (ESEO) in Angers from 2019 to 2022.



Gilbert KABOURÉ is an electronics student-engineer at École Supérieure d'Électronique de l'Ouest (ESEO) in Angers from 2019 to 2022.



Nathan SAUGER is an electronics student-engineer at École Supérieure d'Électronique de l'Ouest (ESEO) in Angers from 2019 to 2022.



Abdelaziz HAMDOUN received the Ph.D. degree in signal processing and telecommunications from the University of Rennes 1, Rennes, France in Cotutelle with Carlton University, Canada. He is an Associate professor at École Supérieure d'Électronique de l'Ouest (ESEO) in Angers, member of RF-EMC research group.



Mohamed LATRACH (IEEE Member and URSI-France Member) received the Ph.D. degree in electronics from the University of Limoges, Limoges, France. He is a Professor of microwave engineering at École Supérieure d'Électronique de l'Ouest (ESEO), Angers, France. He is a founding member of the RF-EMC research group, Angers and Research Associate at the IETR, University of Rennes 1.

His main research interests are in the area of design and analysis of various antenna types, metamaterials, hybrid and MMIC circuits, wireless sensors, RFID, IoT, wireless power transfer and energy harvesting.

Mohamed LATRACH has supervised several doctoral, postdoctoral and master/engineer students. He has many publications and book chapters in the RF and microwave fields. He also holds three patents.

He serves as a reviewer for various journals and congress. He has delivered numerous invited presentations and has participated in many projects.